

Attention In Geometry: An Adaptive Density Field (ADF) with FAISS-Accelerated Spatial Attention

Zhaowen Fan

January 13, 2026

Abstract

Spatial computation in geographic and urban systems increasingly demands scalable mechanisms for aggregating local influence under metric constraints. Classical approaches such as kernel density estimation [13] and spatial interpolation either rely on global summation or treat approximation solely as an implementation concern, limiting their interpretability and scalability in large-scale settings. This work introduces **Adaptive (Attention) Density Fields (ADF)**, a geometric attention framework that formulates spatial aggregation as a query-conditioned, metric-induced attention operator in continuous space. Given a set of spatial points with associated scalar scores, ADF constructs a local adaptive Gaussian mixture centered at the query's nearest neighbors, where kernel bandwidths are modulated by point-specific scores. Approximate nearest-neighbor search, implemented via FAISS [9] inverted file indices, is treated as an intrinsic component of the attention mechanism, enabling scalable execution while preserving locality. ADF bridges concepts from adaptive kernel methods and attention mechanisms by reinterpreting spatial influence as geometry-preserving attention, grounded directly in physical distance rather than learnt latent projections. The framework is formulation-level rather than algorithm-specific, allowing flexible kernel choices, score-to-bandwidth mappings, and approximation parameters. As such, ADF provides a unifying perspective on spatial influence modeling that emphasizes structure, scalability, and geometric interpretability, with relevance to geographic information systems, urban analysis, and spatial machine learning.

This manuscript is a preprint and has not undergone peer review.

1. Introduction

Large-scale spatial analysis increasingly involves aggregating millions of spatially distributed points of interest (POIs), each associated with heterogeneous influence scores. A common goal is to evaluate a continuous influence field

$F(x)$ that reflects the accumulated effect of nearby points under physical distance constraints. However, naive kernel-based summation over all points is computationally infeasible at scale, and classical spatial interpolation methods often treat approximation purely as an implementation concern rather than a structural component of the model.

This work proposes a geometric attention framework for scalable continuous spatial aggregation. Instead of viewing spatial influence as a global density estimation problem, we formulate it as a query-conditioned, metric-induced attention operator in continuous space. Locality, sparsity, and approximation are treated as intrinsic to the formulation, rather than as post hoc accelerations.

This perspective is related in spirit to kernelized and geometry-aware attention mechanisms, but differs in that attention weights are induced directly by physical distance rather than learned projections.

[3] [5]

Given a set of POIs with associated scalar scores, the framework proceeds as follows:

- Map POIs from geodetic (λ, φ, h) to ECEF $\mathbf{x} \in \mathbb{R}^3$;
- Associate each POI with a scalar score s_i representing application-dependent influence;
- Construct an inverted file (IVF) index to accelerate approximate k -nearest-neighbor (k-NN) search in 3D;
- For any query location \mathbf{x} :
 - retrieve its k nearest neighbors,
 - define a Gaussian kernel centered at each neighbor, with bandwidth modulated by its score,
 - aggregate the weighted kernel contributions.

The resulting field $F(\mathbf{x})$ constitutes an *adaptive Gaussian density/intensity field* (ADF): a finite, query-dependent Gaussian mixture that enables scalable evaluation of continuous spatial influence over millions of points with sublinear query complexity.

Importantly, this work focuses on the formulation of geometric attention for spatial aggregation rather than any single algorithmic instantiation. The choice of kernel family, score-to-bandwidth mapping, normalization, and approximation parameters are treated as design degrees of freedom. The emphasis is on the structural decomposition of spatial attention—query-conditioned neighbor selection, metric-grounded weighting, and efficient execution—providing a unifying perspective on adaptive kernel methods, spatial indexing, and attention mechanisms in continuous space.

2. Framework

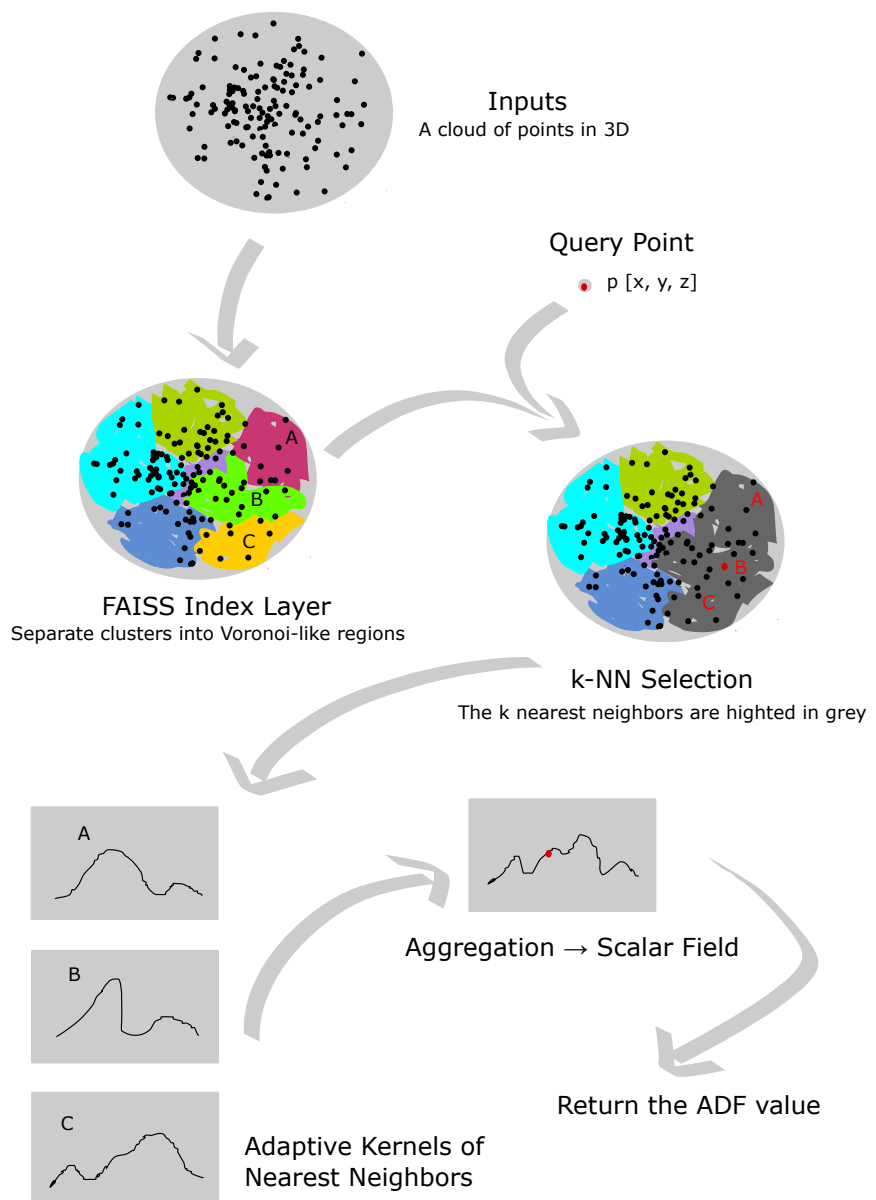


Figure 1: An overview of the proposed framework

2.1. Overview

The Adaptive Density Field (ADF) is a geometric attention operator defined over continuous three-dimensional space. Given a set of spatial points of interest (POIs) with associated scalar scores, ADF constructs a continuous influence field by aggregating local contributions from nearby points.

For each query location, ADF performs a query-conditioned neighbor selection using an approximate k-NN search, followed by a score-modulated kernel weighting in metric space. The aggregation is explicitly localized, sparse, and adaptive, with kernel bandwidths determined by POI scores rather than fixed global parameters.

To ensure scalability to larger datasets, ADF integrates approximate nearest-neighbor search via FAISS inverted file indices, reducing per query complexity from linear to sublinear in the number of POIs. The resulting operator produces a continuous scalar field that can be evaluated at arbitrary spatial locations and serves as a geometry-preserving attention mechanism grounded in physical distance.

2.2. Data Preparation

Suggested data structures: positions and scores In the experiments, POIs are derived from a physics-informed trajectory analysis pipeline that detects anomalous motion based on time-normalized Mahalanobis [11] residuals. Each POI is associated with a spatial location and a scalar score reflecting deviation magnitude. The details of this pipeline are not central to the ADF formulation and are therefore omitted; ADF operates on arbitrary spatial point sets with associated scores, defined as follows:

- $\mathbf{x}_i \in \mathbb{R}^3$: ECEF position of POI i
- s_i : score (weight) of POI i Formally:

$$\{\mathbf{x}_i, s_i\}_{i=1}^n$$

with:

$$\mathbf{x}_i \in \mathbb{R}^3, \quad s_i \in \mathbb{R}.$$

The score s_i represents an application-dependent measure of influence, saliency, or importance, and its semantic interpretation is not constrained by the ADF formulation.

2.3. Methodology

With the POI data, we can perform the ADF construction with the following method:

2.3.1. FAISS IVF Index: Accelerating Neighbor Search For each POI data we imported, we assign the IVF index [8] , mathematically:

Training:

- FAISS runs k-means with $n_{\text{list}} = 4096$ clusters in \mathbb{R}^3 .
- It learns centroids $\{\mathbf{c}_j\}_{j=1}^{4096}$.

$$\min_{\{\mathbf{c}_j\}} \sum_{i=1}^n \min_{1 \leq j \leq 4096} \|\mathbf{x}_i - \mathbf{c}_j\|^2. \quad (1)$$

Assignment: Each vector \mathbf{x}_i is assigned to its nearest centroid:

$$\ell(i) = \arg \min_{1 \leq j \leq 4096} \|\mathbf{x}_i - \mathbf{c}_j\|^2. \quad (2)$$

and it is stored in *inverted list* $L_{\ell(i)}$.

Search: For a query \mathbf{x} , FAISS finds the 16 nearest centroids:

$$j_1, \dots, j_{16} = \text{indices of the 16 closest } \mathbf{c}_j \text{ to } \mathbf{x}.$$

and Searches only in the union of lists:

$$L_{j_1} \cup \dots \cup L_{j_{16}}$$

2.3.2. ADF model: an adaptive gaussian mixture

Neighbor search For a query point $\mathbf{x} \in \mathbb{R}^3$ FAISS returns indices:

$$\{i_1, \dots, i_k\} = \text{k-NN}_{\text{IVF}}(\mathbf{x}) \quad (3)$$

in approximate nearest-neighbor sense. Then set:

- Neighbor positions:

$$\mathbf{x}_{i_j} \in \mathbb{R}^3$$
- Neighbor scores:

$$s_{i_j}$$

Differences Mathematically, for each neighbor $j = 1 \dots k$:

$$\mathbf{d}_j = \mathbf{x}_{i_j} - \mathbf{x} = \begin{bmatrix} x_{i_j,1} - x_1 \\ x_{i_j,2} - x_2 \\ x_{i_j,3} - x_3 \end{bmatrix} \in \mathbb{R}^3. \quad (4)$$

Adaptive Bandwidth For each neighbor j :

$$\sigma_j = \frac{\sigma_0}{s_{i_j} + 10^{-6}}. \quad (5)$$

The $\epsilon = 10^{-6}$ term ensures numerical stability and avoids singular bandwidths. Therefore:

- High score $s_{i_j} \Rightarrow$ smaller $\sigma_j \Rightarrow$ more peaked kernel.
- Low score $s_{i_j} \Rightarrow$ larger $\sigma_j \Rightarrow$ broader kernel. This is why it's *adaptive*: kernel width depends on the score. Then for each j we have:

$$\text{inv_var}_j = \frac{1}{\sigma_j^2}. \quad (6)$$

NOTE: The specific functional form relating scores to bandwidths (Eq. 5) is a *design choice*, not a defining property of ADF. ADF is defined by (i) query-conditioned neighbor selection, (ii) metric-induced kernel weighting, and (iii) scalable approximate execution. Any monotonic or learned score-to-bandwidth mapping may be substituted without altering the underlying framework. *This work focuses on the general framework of adaptive, score-modulated kernels; alternative monotonic mappings or learned parameterizations can be substituted without altering the structure of ADF.*

Quadratic Form (Mahalanobis Distance Squared) From equation 4 (Eq. 4) we can derive the componentwise square:

$$(\mathbf{d}_j)^2 = \begin{bmatrix} (x_{i_j,1} - x_1)^2 \\ (x_{i_j,2} - x_2)^2 \\ (x_{i_j,3} - x_3)^2 \end{bmatrix} \quad (7)$$

Additionally, we have an array with shape $(k, 1)$, broadcasts inv_var_j across the 3 dimensions. So for each neighbor j :

$$\text{quad}_j = \sum_{d=1}^3 (x_{i_j,d} - x_d)^2 \cdot \frac{1}{\sigma_j^2} = \frac{\|\mathbf{x}_{i_j} - \mathbf{x}\|^2}{\sigma_j^2}. \quad (8)$$

This is exactly the *Mahalanobis distance squared* for an isotropic Gaussian with variance σ_j^2 :

$$\text{quad}_j = (\mathbf{x} - \mathbf{x}_{i_j})^T \Sigma_j^{-1} (\mathbf{x} - \mathbf{x}_{i_j}), \quad (9)$$

where

$$\Sigma_j = \sigma_j^2 I_3, \quad \Sigma_j^{-1} = \frac{1}{\sigma_j^2} I_3.$$

Gaussian Kernel and ADF Value For each neighbor j , the kernel contribution is:

$$K_j(\mathbf{x}) = \exp\left(-\frac{1}{2}\text{quad}_j\right) = \exp\left(-\frac{1}{2}\frac{\|\mathbf{x} - \mathbf{x}_{i_j}\|^2}{\sigma_j^2}\right). \quad (10)$$

In this work, we assume isotropic kernels with $\Sigma_j = \sigma_j^2 I_3$. And anisotropic kernels are discussed as a future extension. Then the *ADF value* at \mathbf{x} is:

$$F(\mathbf{x}) = \sum_{j=1}^k s_{i_j} K_j(\mathbf{x}) = \sum_{j=1}^k s_{i_j} \exp\left(-\frac{1}{2}\frac{\|\mathbf{x} - \mathbf{x}_{i_j}\|^2}{\sigma_j^2}\right). \quad (11)$$

Therefore, we claim that ADF is a *finite Gaussian mixture* [2] centered at the nearest neighbors, with:

- centers \mathbf{x}_{i_j}
- weights s_{i_j}
- bandwidths $\sigma_j = \sigma_0/(s_{i_j} + 10^{-6})$.

Assume (i) $s_i \geq 0$, or s_i is transformed via $s_i \leftarrow \text{softplus}(s_i)$, (ii) σ_0 or the score-to-bandwidth mapping can be learned via gradient descent, (iii) σ_0 has units of meters and controls the physical spatial influence scale.

This can be interpreted as an *adaptive kernel density / intensity field* in 3D ECEF space.

The contribution of this work lies in the formulation of ADF as a geometric attention mechanism with scalable execution. Kernel choices, bandwidth parameterizations, and score transformations are intentionally left flexible to emphasize the generality of the framework.

2.4. Computational complexity analysis

2.4.1. Time complexity

Without FAISS:

$$O(n) \text{ per query}$$

With FAISS IVF:

$$O(n_{\text{probe}} \cdot \frac{n}{n_{\text{list}}} + k)$$

2.4.2. Memory Complexity

$$O(n)$$

dominated by the inverted lists.

2.5. Evaluation

2.5.1. Approximation Error Acknowledgement Since FAISS IVF performs approximate nearest-neighbor search, $ADF(\mathbf{x})$ is an approximation of the full kernel sum. However, locality of the Gaussian kernel ensures distant errors contribute negligibly. In practice, approximation quality is controlled by n_{probe} and k .

2.5.2. Evaluating ADF at all POIs For each POI position \mathbf{x}_i :

$$ADF_i = F(\mathbf{x}_i) = \sum_{j=1}^k s_{i_j} \exp\left(-\frac{1}{2} \frac{\|\mathbf{x}_i - \mathbf{x}_{i_j}\|^2}{\sigma_j^2}\right), \quad (12)$$

where $\{i_1, \dots, i_k\}$ are the k -nearest neighbors of \mathbf{x}_i according to the IVF-accelerated FAISS search. So the final result is a *scalar ADF field* defined on all your POIs:

$$\mathbf{x}_i \mapsto ADF_i.$$

2.6. Comparison

2.6.1. Relation to Kernel Density Estimation Classical KDE [13] evaluates a global sum over all points using fixed or locally adaptive bandwidths. In contrast, ADF is explicitly defined as a local, query-dependent aggregation mechanism with bounded support induced by k-NN search. Moreover, ADF is interpreted as a spatial attention operator rather than a probability density estimator, and is designed for scalable execution via approximate nearest-neighbor indices.

ANN-accelerated KDE methods primarily focus on speeding up density estimation. ADF differs in that approximation is not merely an implementation detail, but an explicit component of the attention mechanism, where k-NN selection corresponds to top-k attention pruning.

2.6.2 Relation to the Attention Mechanism [15]

While attention mechanisms are typically defined over discrete tokens in a learned latent space, ADF operates directly in continuous metric space. Similarity is induced by physical distance rather than learned projections, and attention weights arise from energy-based kernels instead of normalized dot products. As a result, ADF should be viewed not as a rebranding of Transformer attention, but as a geometric generalization of attention to continuous spatial domains.

Table 1 Here's the direct correspondence:

ADF Component	Attention Component	Meaning
Query point x	Query vector Q	“Where should we look?”
POI positions x_i	Key vectors K_i	“What do we compare against?”
POI scores s_i	Value vectors V_i	“What do we aggregate?”
Gaussian kernel	(Unnormalized) attention weights	“How strongly do we attend to each neighbor?”
FAISS k-NN	Top-k attention pruning	“Only attend to the nearest keys.”

This correspondence is structural rather than metaphorical:

ADF satisfies the abstract definition of attention as a metric-induced aggregation mechanism over continuous space.

The attention analogy is used as a structural lens rather than a claim of architectural novelty.

Unlike Transformer’s attention, which operates in a learned latent space, ADF attention is geometry-preserving and grounded in physical distance. No projection matrices are required; relevance emerges directly from the spatial metric. Moreover, ADF attention is metric-induced and geometry-preserving, requiring no learned projection matrices.

2.6.3 Why This Matters The suggested ADF is a *geometric attention*:

- Query = location where you want influence
- Keys = POI positions
- Values = POI scores
- Kernel = attention weights
- FAISS = top-k attention pruning

This built a *spatial attention mechanism*.

While ADF shares mathematical components with adaptive KDE and ANN-accelerated density estimation, its contribution is not a new kernel estimator per se. Instead, ADF explicitly formulates these components as a geometric attention operator, where approximation, sparsification, and metric structure are intrinsic to the definition rather than implementation details.

Importantly, the attention analogy is used as a structural lens rather than a claim of architectural novelty. ADF does not seek to replace

or subsume Transformer-style attention, but to extend the abstract notion of query-conditioned weighted aggregation to continuous metric spaces.

Overall, ADF should be understood as a framework-level operator rather than a fixed algorithm, with emphasis on structure, scalability, and geometric grounding.

3. Implementation and results

Given a large set of aircraft trajectories, local motion irregularities are first detected as Points of interest (POIs). These POIs are sparse, noisy, and heterogeneous. We aim to aggregate them into a continuous spatial field to reveal Zones of Influence (ZOIs): regions where systematic maneuvering, airspace structure, or control-induced behavior recurrently concentrates.

In many spatial decision problems (e.g., flight routing, navigation, risk exposure), the agent does not respond to absolute field intensity, but to relative dominance along its trajectory. Zones of Influence (ZOIs) are therefore introduced as *trajectory-conditioned dominance regions*, representing spatial areas where the accumulated influence field locally dominates competing influences relative to the agent’s path.

3.1. Study area and data description

We used a nationwide flight trajectory dataset over mainland China for two multi-periods: 2024-11-10 to 2024-11-22 and 2024-12-05 to 2024-12-15 to extract the POIs. There are a total of 1.8 millions of POIs extracted from the dataset using the motion-based procedure described in Section 3.2.

For the case study on trajectory-conditioned ZOIs, we selected a single day and airport: the Chengdu Shuangliu airport (CTU) on 2024-12-16. All trajectories intersecting the Chengdu region on that day were used to construct a local example of the Adaptive Density Field (ADF) and to illustrate ZOI extraction along individual flights.

The ADF framework is not restricted to flight trajectories and can be instantiated in any domain where localized motion irregularities or events are observed. Likewise, the POI definition is not universal; the construction adopted here is a concrete example tailored to aircraft motion.

3.2. POI construction

To collect the POI data, we applied a mixture of motion-based POI detection methods, detailed in the Appendix. However, POIs are derived from trajectory segments where a physics-based motion model fails to predict future positions accurately. The processing pipeline operates at the individual flight level. For

each flight, raw WGS-84 positions (longitude, latitude, altitude) are first converted to a local East–North–Up (ENU) coordinate system. The trajectory is then represented as a dictionary keyed by flight identifier, with three aligned time series:

- **coords:** longitude, latitude, altitude
- **vel:** velocity components (velocity on each axis)
- **dt:** timestamp interval

To estimate future aircraft positions, I applied a *physics-based interpolation model* that blends two motion predictors:

1. **Constant-Acceleration (CA) model:** reliable for nearly straight trajectories
2. **Cubic Hermite Spline interpolation:** smooth and accurate for curved motion

the blending weight is determined by the *local curvature* of the trajectory [10]: Low curvature indicates motion is nearly straight, hence CA weights more, and vice versa. This adaptive combination produces a more stable and realistic prediction thanm using either method alone.

To evaluate the quality of the predicted positions, I compute a *time-normalized Mahalanobis loss* (This metric captures both the magnitude and directional structure of prediction errors.) for each flight. This metric captures not only the magnitude of prediction errors but also their *directional structure, covariance, and temporal spacing*. After computing the time-normalized Mahalanobis loss for each flight, the next step is to identify *Points of Interest (POIs)*—locations where the prediction error is unusually high [4]. These points often correspond to sharp maneuvers, abnormal motion, or sensor irregularities, and they serve as valuable markers for downstream analysis.

However, in this case, a POI does not necessarily correspond to an actual infrastructure feature; it simply marks a point where the motion deviates significantly from our prediction. It can be regard as an example tailored POI definition under certain circumstances.

Later we normalize the loss scores and filter the POI with a threshold and exported the data into csv format.

3.3. ADF construction

We instantiated the ADF framework on the nationwide POI dataset by specifying the coordinate system, kernel parameterizations, and neighbor search configurations. All POI locations were converted from WGS84 geodetic coordinates to Earth-Centered, Earth-Fixed (ECEF) Cartesian coordinates to ensure metric consistency. POI scores were treated as non-negative scalar probability attention values and were used directly without additionaly normalization.

For the scalable neighbor retrieval, a FAISS inverted file (IVF) index was introduced and constructed over the ECEF coordinates. The index was trained with 4096 clusters (2^{12}) clusters, and queries probed the 16 nearest clusters. For each query point the top $k = 100$ approximate nearest neighbors were retrieved. The global spatial scale parameter was fixed to $\sigma_0 = 500$ meters for all experiments. ADF values were evaluated using the formulation defined in Section 2, without further modification.

Unless otherwise stated, these parameter choices were held constant throughout the case study.

3.4. Field evaluation

To analyze the ADF along individual trajectories in Chengdu, we:

1. **Convert the coordinates:** transform all points from geodetic to ECEF.
2. **Evaluate ADF:** compute $ADF(x_t)$ at each trajectory point x_t using the FAISS-accelerated framework.
3. **Re-attach geodetic coordinates:** join ADF values back to (lon, lat, alt) for downstream analysis.

This allows us to examine how aircraft trajectories intersect regions of concentrated POIs.

3.5. ZOI extraction

Given the ADF evaluated along a trajectory, we extract Zones of Influence (ZOIs) as segments where the field intensity dominates a baseline [17] defined by the flight’s own experience. Let $\{F_t\}$ denote the sequence of ADF values along a single trajectory. We define a robust baseline level as the trajectory-wise median [12]:

$$F_{base} = median_t(F_t)$$

A point t is labeled as belonging to a ZOI if

$$F_t \geq \alpha F_{base}$$

where $\alpha > 1$ is a dominance factor. In the Chengdu case study, we set $\alpha = 1.3$, chosen empirically to balance sensitivity and specificity in detecting high-density segments along individual trajectories. The resulting binary mask partitions the trajectory into ZOI and non-ZOI segments. Trajectories primarily in low-density regions may still exhibit short ZOIs, while trajectories in busy airspace require higher ADF values to exceed the baseline.

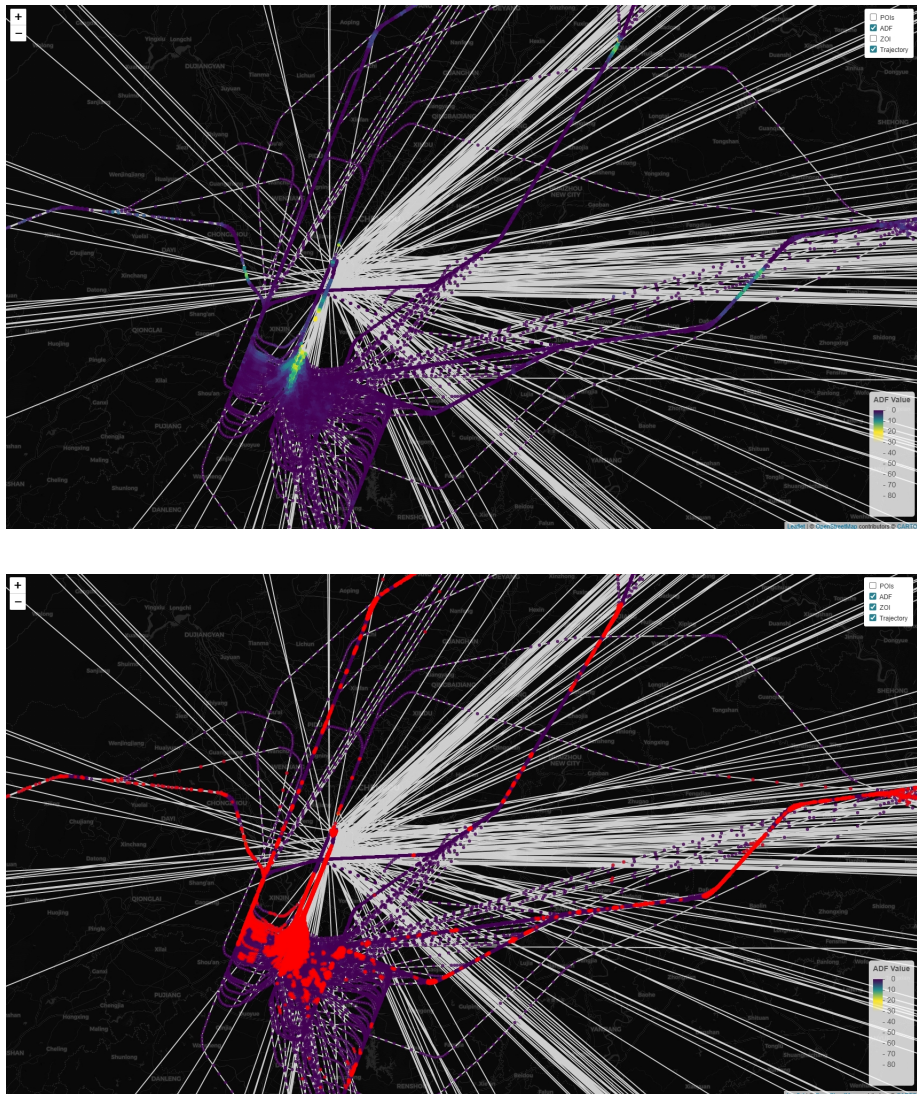


Figure 2: Trajectory ADF analysis and ZOI extraction

Visualization To illustrate the ADF and ZOI extraction:

- Trajectories are rendered as white lines, tracing the actual flight paths through the airspace.
- Red dots mark the extracted Zones of Influence (ZOIs)—trajectory points where the ADF value exceeds the dominance threshold relative to the flight’s own baseline.
- The remaining trajectory points are colored by their Adaptive Density Field (ADF) values (within range 0~30), using a continuous colormap from blue (low intensity) to red (high intensity), with values ranging from 0 to 80.
- Layered maps allow toggling between POIs, ADF, ZOIs, and trajectory paths, enabling flexible inspection of each component.

These visualizations demonstrate the relationship between the continuous ADF field and trajectory-conditioned ZOIs. High-ADF segments generally coincide with operationally significant areas such as approach corridors, holding patterns, and vectoring zones in the Chengdu terminal. ZOI points, highlighted in red, mark locations where the trajectory locally exceeds its baseline field intensity; some of these points overlap dense ADF regions, representing recurrent maneuvering, while others appear in otherwise sparse areas, potentially reflecting transient anomalies, unique pilot actions, or data artifacts. By layering ADF intensity, ZOI labels, and raw POIs, the visualization distinguishes between structurally recurrent behavior and isolated events, offering a nuanced perspective on spatial influence and motion irregularities.

4. Discussion

The proposed Adaptive Density Field (ADF) framework provides a flexible, scalable mechanism for aggregating sparse, heterogeneous points of interest (POIs) into a continuous spatial field. By coupling trajectory-conditioned analysis with ZOI extraction as a downstream instantiation of ADF, this methodology captures both globally recurrent patterns and locally significant deviations.

4.1. Future application and extensions

1. **Operational Airspace Management:** The ADF-ZOI pipeline we presented in the example implementation section could assist air traffic controllers in identifying target regions depending on the specific POI definition, such as regions of frequent maneuvering or congestion, enabling data-driven decisions for route planning, holding pattern optimization, and as well as safety monitoring.
2. **Predictive Trajectory Analysis:** Beyond post-hoc evaluation, the framework can be integrated with predictive models for trajectory planning, anomaly detection, or risk exposure assessment. By defining

the POIs, it is possible to derive trajectory-conditioned ZOIs to provide adaptive thresholds for identifying unusual events relative to expected motion patterns.

3. **Cross-Domain Applicability:** While this study focuses on aircraft trajectories due to the initial problem setting, the methodology is domain-agnostic. Any scenario involving spatiotemporal events, as long as the spatial characteristics are stable and fixed (in other words, not dynamic), such as maritime traffic, pedestrian movement, vehicle flows, or wildlife tracking – we expect ADF-based spatial attention is able to identify zones of concentrated activities.
4. **Integration with Semantic Context:** Future work could embed semantic labels, such as airspace type, weather conditions, or operational procedures, into the ADF formulation, yielding geo-semantic density fields. This way, interestingly, aligns even more closely with the application of attention mechanism in spatiotemporal analysis.
5. **Real-Time Applications:** With optimizations to indexing, neighbor search, or GPU-accelerated computation, the ADF framework could support near-real-time monitoring of live trajectories in drones, robotics, and other autonomous systems, allowing dynamic ZOI identification and interactive visualization for operational decision-making.

4.2. Methodological Reflections

- The trajectory-conditioned approach ensures that high-density areas are interpreted relative to the agent’s path, avoiding misleading conclusions based solely on absolute field intensity.
- Parameter choices, such as kernel bandwidth and dominance factor, influence sensitivity and specificity; future studies could explore adaptive or data-driven tuning to optimize ZOI detection across heterogeneous datasets.
- Visualization remains crucial for interpretation: layered maps combining POIs, ADF intensity, and ZOI labels provide immediate insight into both recurrent behavior and outlier events, but higher-dimensional visualizations or interactive dashboards could further enhance understanding.
- This study represents a conceptual framework, and some details may therefore be approximate, incomplete, or provisional.

5. Conclusion

This work introduces Adaptive Density Fields (ADF) as a formulation-level geometric attention operator for scalable aggregation of sparse spatial events in continuous metric space. By defining spatial influence through query-conditioned

neighbor selection, score-modulated kernel weighting, and approximate nearest-neighbor execution, ADF reframes adaptive kernel aggregation as an intrinsic form of geometry-preserving attention rather than a purely statistical estimator. The primary contribution lies not in a specific kernel choice or application, but in the structural decomposition of spatial aggregation: locality induced by k-NN attention, metric-grounded weighting, and approximation treated as a defining component of the operator. This perspective unifies ideas from adaptive kernel methods, spatial indexing, and attention mechanisms under a common geometric framework that scales to millions of points while remaining interpretable. To demonstrate the utility of this formulation, we presented an example instantiation in the context of aircraft trajectory analysis. Motion-derived Points of Interest were aggregated into a continuous ADF, and trajectory-conditioned Zones of Influence (ZOIs) were extracted using a relative dominance criterion along individual paths. The Chengdu case study illustrates how the resulting fields reveal recurrent airspace structures while distinguishing localized, trajectory-specific deviations. Beyond aviation, the ADF framework is domain-agnostic and applicable to a wide range of spatial and spatiotemporal settings, including urban mobility, maritime traffic, robotics, and environmental monitoring. Future work will explore semantic augmentation of the field, adaptive parameter learning, anisotropic kernels, and real-time deployment, further extending the applicability of geometric attention in continuous spatial systems. Overall, ADF provides a robust and extensible foundation for scalable, interpretable spatial attention, bridging geometric structure and efficient computation in complex spatial environments.

References

- [1] Yaakov Bar-Shalom, X Rong Li, and Thiagalingam Kirubarajan. *Estimation with applications to tracking and navigation: theory algorithms and software*. John Wiley & Sons, 2001.
- [2] Christopher M Bishop and Nasser M Nasrabadi. *Pattern recognition and machine learning*, volume 4. Springer, 2006.
- [3] Michael M Bronstein, Joan Bruna, Taco Cohen, and Petar Veličković. Geometric deep learning: Grids, groups, graphs, geodesics, and gauges. *arXiv preprint arXiv:2104.13478*, 2021.
- [4] Varun Chandola, Arindam Banerjee, and Vipin Kumar. Anomaly detection: A survey. *ACM computing surveys (CSUR)*, 41(3):1–58, 2009.
- [5] Krzysztof Choromanski, Valerii Likhoshesterov, David Dohan, Xingyou Song, Andreea Gane, Tamas Sarlos, Peter Hawkins, Jared Davis, Afroz Mohiuddin, Lukasz Kaiser, et al. Rethinking attention with performers. *arXiv preprint arXiv:2009.14794*, 2020.

- [6] Carl De Boor and Carl De Boor. *A practical guide to splines*, volume 27. Springer New York, 1978.
- [7] Bernhard Hofmann-Wellenhof, Herbert Lichtenegger, and James Collins. *Global positioning system: theory and practice*. Springer Science & Business Media, 2012.
- [8] Hervé Jégou, Matthijs Douze, and Cordelia Schmid. Product quantization for nearest neighbor search. *IEEE transactions on pattern analysis and machine intelligence*, 33(1):117–128, 2011.
- [9] Jeff Johnson, Matthijs Douze, and Hervé Jégou. Billion-scale similarity search with gpus. *IEEE Transactions on Big Data*, 2017.
- [10] Jae-Gil Lee, Jiawei Han, and Kyu-Young Whang. Trajectory clustering: a partition-and-group framework. In *Proceedings of the 2007 ACM SIGMOD international conference on Management of data*, pages 593–604, 2007.
- [11] P. C. Mahalanobis. On the generalized distance in statistics. *Proceedings of the National Institute of Sciences of India*, 1936.
- [12] Peter J Rousseeuw and Christophe Croux. Alternatives to the median absolute deviation. *Journal of the American Statistical association*, 88(424):1273–1283, 1993.
- [13] B. W. Silverman. *Density Estimation for Statistics and Data Analysis*. Chapman and Hall, 1986.
- [14] Andrei N Tikhonov. Solution of incorrectly formulated problems and the regularization method. *Sov Dok*, 4:1035–1038, 1963.
- [15] Ashish Vaswani et al. Attention is all you need. *Advances in Neural Information Processing Systems*, 2017.
- [16] Pauli Virtanen, Ralf Gommers, Travis E Oliphant, Matt Haberland, Tyler Reddy, David Cournapeau, Evgeni Burovski, Pearu Peterson, Warren Weckesser, Jonathan Bright, et al. Scipy 1.0: fundamental algorithms for scientific computing in python. *Nature methods*, 17(3):261–272, 2020.
- [17] Yu Zheng. Trajectory data mining: an overview. *ACM Transactions on Intelligent Systems and Technology (TIST)*, 6(3):1–41, 2015.

Appendix: Physics-informed Trajectory POI Detection Pipeline

The appendix provides implementation-level details and mathematical formulations supporting the methods described in the main text. Citations follow the same reference list as the main body.

1 Preprocessing the Flight Data

1.1 Coordinate Conversion [7]: WGS84 Geodetic to ECEF Given:

- latitude φ (rad)
- longitude λ (rad)
- ellipsoidal height h (m)
- WGS84 parameters:
 - semi-major axis $a = 6378137.0$
 - flattening rate $f = \frac{1}{298.257223563}$
 - first eccentricity squared $e^2 = 6.69437999014 \times 10^{-3}$

First compute the prime vertical radius of curvature:

$$N(\varphi) = \frac{a}{\sqrt{1 - e^2 \sin^2 \varphi}} \quad (1.1.1)$$

Then ECEF coordinates (x, y, z) :

$$\begin{aligned} x &= (N(\varphi) + h) \cos \varphi \cos \lambda \\ y &= (N(\varphi) + h) \cos \varphi \sin \lambda \\ z &= (N(\varphi)(1 - e^2) + h) \sin \varphi \end{aligned} \quad (1.1.2)$$

Hence we get the ENU coordinates.

1.2 Coordinate Conversion: ECEF to ENU Conversion Pick a reference point (the origin of the local ENU frame in this case) with geodetic coordinates $(\varphi_0, \lambda_0, h_0)$, and compute its ECEF coordinates (x_0, y_0, z_0) using the same equations as above.

For any point with ECEF (x, y, z) , define the difference vector:

$$\begin{bmatrix} \Delta x \\ \Delta y \\ \Delta z \end{bmatrix} = \begin{bmatrix} x - x_0 \\ y - y_0 \\ z - z_0 \end{bmatrix} \quad (1.2.1)$$

And given the Rotation matrix and ENU coordinate at reference $(\varphi_0, \lambda_0, h_0)$:

$$\mathbf{R} = \begin{bmatrix} \sin \varphi_0 & \cos \varphi_0 & 0 \\ \cos \varphi_0 \cdot \sin \lambda_0 & -\sin \varphi_0 \cdot \sin \lambda_0 & \cos \lambda_0 \\ \cos \varphi_0 \cdot \cos \lambda_0 & \sin \varphi_0 \cdot \cos \lambda_0 & \sin \lambda_0 \end{bmatrix} \quad (1.2.2)$$

Therefore we have the calculation:

$$\begin{bmatrix} E \\ N \\ U \end{bmatrix} = \begin{bmatrix} \Delta x \\ \Delta y \\ \Delta z \end{bmatrix} \cdot \mathbf{R} \quad (1.2.3)$$

This is the standard ECEF \rightarrow ENU transformation used in geodesy and navigation.

1.3 Creating a Dictionary To organize per-flight data extracted from each GeoJSON file, we build a dictionary where each flight ID maps to three lists:

- coords — longitude, latitude, altitude
- vel — velocity components
- dt — timestamps

The basic structure looks like this:

```
flights = dict({
    "coords": [],
    "vel": [],
    "dt": []
})
```

In practice, we use a defaultdict so each new flight_id automatically initializes this structure.

2 Position Prediction

To estimate future aircraft positions, I applied a **physics-based interpolation model** that blends two motion predictors:

1. **Constant-Acceleration (CA) model** [1] — reliable for nearly straight trajectories
2. **Cubic Hermite Spline interpolation** [6] — smooth and accurate for curved motion

The spline utilizes local velocity vectors as tangents at each waypoint, providing a geometrically consistent path [16] that complements the CA model's acceleration-based predictions.”

The blending weight is determined by the **local curvature** of the trajectory: -
 Low curvature → motion is nearly straight → CA dominates
 - High curvature → motion bends → spline dominates

This adaptive combination produces a more stable and realistic prediction than using either method alone.

2.1 General Prediction

For each flight:

- Convert raw coordinates into a consistent Cartesian frame
- Compute velocity and approximate acceleration
- Estimate local curvature k using

$$k = \frac{\|\mathbf{v} \times \mathbf{a}\|}{\|\mathbf{v}\|^3} \quad (2.1.1)$$

- Compute a flight-specific smoothing parameter

$$\alpha = \frac{\ln 5}{k_{95}} \quad (2.1.2)$$

where k_{95} is the 95th percentile curvature

- For each timestamp, compute:
 - **Spline prediction** using `CubicHermiteSpline`
 - **Constant-acceleration prediction** - Blend them using $w = e^{-\alpha k}$:

$$\hat{p} = w p_{\text{CA}} + (1 - w) p_{\text{spline}} \quad (2.1.3)$$

This yields a smooth, curvature-aware prediction for each flight.

2.2 Loss Computation To evaluate the quality of the predicted positions, I compute a **time-normalized Mahalanobis loss** for each flight. This metric captures not only the magnitude of prediction errors but also their **directional structure, covariance, and temporal spacing**.

The loss is computed in four main steps:

1. Extract Prediction Residuals

For each flight, I compare the predicted positions \hat{p}_i with the actual converted coordinates p_i :

$$r_i = \hat{p}_i - p_i \quad (2.2.1)$$

Only interior points are used `[2 : size-2]` to avoid boundary artifacts from the spline and acceleration models.

The residuals are then centered:

$$\tilde{r}_i = r_i - \bar{r} \quad (2.2.2)$$

This removes global bias and ensures the covariance reflects *shape* rather than offset.

2. Estimate Residual Covariance

The covariance of the centered residuals is computed as:

$$\Sigma = \text{Cov}(\tilde{r}) + \lambda I \quad (2.2.3)$$

A small Tikhonov regularization [14] term $\lambda = 10^{-5}$ stabilizes the inversion of Σ , especially for nearly collinear trajectories.

The inverse covariance Σ^{-1} defines the **Mahalanobis geometry** of the error space.

3. Compute Mahalanobis Distance

For each residual vector:

$$d_i = \sqrt{\tilde{r}_i^\top \Sigma^{-1} \tilde{r}_i} \quad (2.2.4)$$

This distance penalizes errors more strongly along directions where the model is normally precise, and less along directions with naturally higher variance.

4. Normalize by Temporal Spacing

Because timestamps are not uniformly spaced, each error is scaled by a time-dependent factor:

$$t_i = \sqrt{\frac{\Delta t_i}{\bar{\Delta t}}} \quad (2.2.5)$$

The final **time-relative Mahalanobis loss** is:

$$L_i = \frac{d_i}{t_i} \quad (2.2.6)$$

This ensures that predictions made over longer time intervals are not unfairly penalized compared to short-interval predictions.

3 POI Detection

After computing the time-normalized Mahalanobis loss for each flight, the next step is to identify **Points of Interest (POIs)**—locations where the prediction error is unusually high. These points often correspond to sharp maneuvers, abnormal motion, or sensor irregularities, and they serve as valuable markers for downstream analysis.

However, a POI does not always represent an actual infrastructure feature; it simply marks a point where the motion deviates significantly.

The POI detection pipeline consists of three main stages:

3.1 Normalize the Loss Scores For each flight, the Mahalanobis losses are rescaled to the interval $[0, 1]$:

$$s_i = \frac{L_i - \min(L)}{\max(L) - \min(L) + \varepsilon} \quad (3.1)$$

This normalization ensures that POI detection is **relative to each flight's own dynamics**, making the method robust to differences in scale, speed, or noise across flights.

3.2 Thresholding Here, I introduced an element called POI score, which indicates how anomalous each point is relative to the rest of the flight.

A point is flagged as a POI if its normalized score exceeds a fixed threshold:

$$s_i \geq 0.75 \quad (3.2)$$

This threshold captures the upper quartile of anomalous behavior while avoiding excessive false positives.

It can be adjusted depending on the desired sensitivity of the detection process.

3.3 Export POIs to CSV Each detected POI is stored with:

- flight ID
- point index
- longitude, latitude, altitude
- POI score

All POIs are aggregated into a Pandas DataFrame and exported as a CSV file, enabling further visualization, inspection, or integration into downstream workflows.